HIGH-RESOLUTION IMAGING OF THE DOUBLE QSO 2345+007

NICHOLAS WEIR AND S. DJORGOVSKI[1]

Palomar Observatory, California Institute of Technology, Pasadena, California 91125

Received 26 June 1990; revised 14 September 1990

ABSTRACT

We present raw and maximum entropy restored images of the quasar pair (gravitational lens candidate) 2345 + 007 A and B. Restorations are performed using an implementation of the Gull–Skilling MEMSYS-3 package of maximum entropy method subroutines designed to achieve subpixel resolution in certain data regimes. Extensive simulations of our data imply that we are able to detect structure in the restored images down to the 0.4″ level. Using this method, we qualitatively confirm that component B is resolved and, at least at visual and red wavelengths, elongated in a direction almost perpendicular to the line joining A and B. We also find evidence for a color difference and variation in the magnitude difference between the two components. We believe these data, in conjunction with recent spectroscopic results, more likely favor the multiple quasar rather than gravitational lens interpretation of the objects.

1. INTRODUCTION

A correct physical explanation of the QSO pair 2345 + 007 A, B is of interest to astrophysicists for a variety of reasons, chief among them its implication for the sizes of Lyman α forest clouds and the distribution of dark matter in the universe. Whether the QSOs are physically distinct or lensed images of the same object significantly affects the inferred size limits on the clouds, with the limit being much larger in the event of no lensing (Foltz *et al.* 1984; Steidel & Sargent 1990). If the pair *is* the result of a lens, the lack of detection of an intervening galaxy or cluster places constraints on the nature of the lensing dark matter and its distribution (Tyson *et al.* 1986).

Previous efforts to uncover the nature of 2345 + 007 since its discovery by Weedman *et al.* (1982) include spectral studies by Foltz *et al.* (1984) and Steidel & Sargent (1990), photometry and imaging by Sol *et al.* (1984) and Tyson *et al.* (1986), and high-resolution imaging by Nieto *et al.* (1988). In this paper we present recent multiband observations of the QSOs, including differential photometry of the two components and maximum entropy restorations of the images for high-resolution morphological analysis.

2. OBSERVATIONS

Our images of the 2345 + 007 field were obtained on the nights of 30 August and 23 September 1989 UT at the Palomar 60 in. telescope using a TI 800×800 CCD and on 6 September 1989 UT at the Palomar 200 in. Hale Telescope using the 4-Shooter camera. The filters we used included Thuan-Gunn *g*, *r*, and *i*, in addition to Johnson *B*. On 30 August, we took one 900 s exposure in *r*. On 6 September, we made images of 400 s in *g*, 300 s in *r*, and 300 s in *i*. On 23 September, exposures of 600 s in *B*, 300 s in *g*, 300 s in *r*, and 300 s in *i* were obtained. The seeing was approximately 1.4″ for the 30 August observation and averaged 1.1″ for the remainder of the images. The pixel scale on the 60 in CCD is 0.246″/pixel, and on the 4-Shooter it is approximately 0.335″/pixel. The data were bias subtracted and flatfielded using standard procedures.

Differential photometry of components A and B was obtained for each image using the DAOPHOT package (Stetson

1987). Two or three unsaturated stars were available in each field for constructing a point-spread function (PSF) template with which the object images were fit to obtain their instrumental magnitudes. The magnitude difference between the components for each of our exposures is listed in Table 1, along with the results of previous authors. Note that our data corroborate the previously observed, marginally redder color of component B, and that there now appears to be a possibility of variability between the objects. In particular, we call attention to the consistently lower magnitude differences we find compared to all previous measurements. In Sec. 5 we discuss a possible explanation for the rather large discrepancy between Steidel & Sargent's (1990) and our measurement at nearly the same epoch.

3. RESTORATIONS

We performed maximum entropy restorations of the three images taken on September 6 on the 200 in. telescope. (The other frames were of insufficient image quality to achieve the desired very high level of resolution.) For our restorations we used MEM, a shell utilizing the MEMSYS-3 package of routines (Gull & Skilling 1989) for maximum entropy reconstruction of arbitrary sets of data. MEM is a modified version

TABLE 1. Magnitude differences for Q2345 + 007 A and B.

Reference	Epoch	Measurement	
Sol *et al.* (1984)	1981.92	ΔU	$= 1.45 \pm 0.06$
		ΔB	$= 1.43 \pm 0.06$
		ΔV	$= 1.43 \pm 0.05$
	1981.98	Δr	$= 1.54 \pm 0.13$
	1982.57	Δr	$= 1.44 \pm 0.15$
	1982.90	Δr	$= 1.41 \pm 0.13$
Nieto *et al.* (1988)	1984.79	ΔV	$= 1.76 \pm 0.05$
Tyson *et al.* (1986)	1984,1985	ΔJ_{ccd}	$= 1.44$
		ΔR	$= 1.39$
		ΔI	$= 1.33$
Steidel & Sargent (1990)	1989.62	Δm_{spect}	$= 1.43 \pm 0.01$
This work	1989.65	ΔB	$= 1.30 \pm 0.14$
		Δg	$= 1.31 \pm 0.07$
		Δr	$= 1.24 \pm 0.06$
		Δi	$= 1.08 \pm 0.06$
	1989.67	Δr	$= 1.28 \pm 0.04$
	1989.69	Δg	$= 1.32 \pm 0.03$
		Δr	$= 1.27 \pm 0.04$
		Δi	$= 1.19 \pm 0.04$

[1] Alfred P. Sloan Foundation Fellow.

of the maximum entropy image restoration system previous-
ly described by Weir (1987) and used in a variety of astro-
nomical applications (e.g., Schild *et al.* 1989). This new
shell allows one to solve for the restored image at subpixel
spatial scales, providing virtually the highest resolution pos-
sible for any given direct image. While a more detailed paper
describing this system is forthcoming (Weir 1991), we brief-
ly describe some of it characteristics below.

The estimation of a PSF is critical to any deconvolution
method, particularly when attempting to extract informa-
tion at the fractional pixel level. For our restorations, we
typically utilize the PSF determined by DAOPHOT from a
composite of stars in the image of interest. To restore to
subpixel spatial scales, this PSF array is expanded via cubic
spline interpolation to the scale desired in the final restora-
tion. After estimating the noise and subtracting the sky value
for each pixel in the data, we begin solving for the restored
image using a perfectly flat array as the initial guess. The
MEM algorithm iterates toward that restored image which
achieves a "suitable" balance between image entropy, assur-
ing smoothness and enhanced resolution via the positivity
constraint, and fidelity to the data when convolved with the
PSF. The new MEMSYS-3 code objectively quantifies and de-
termines what is *the* suitable balance in a fully Bayesian man-
ner, resulting in a purely objective stopping criterion for the
restoration method (Gull & Skilling 1989; Gull 1989; Skill-
ing 1989).

The original data images and the resulting restorations for
the three September 6 observations are plotted in gray scale
in Fig. 1. All unrestored images are displayed such that one
standard deviation below the sky is white, and half the peak
signal value above the sky and greater is black. In the re-
stored images, white corresponds to zero while black repre-
sents greater than 1% of the peak. The insets in each of the
restored images are contour plots of the restored compo-
nents A and B, enlarged by a factor of 3 relative to the gray-
scale plots. The lowest contour in each represents 0.25% of
the peak pixel flux for that object with successive contours
occurring at powers of two times this value. Each image was
restored with three times higher spatial sampling than in the
original data. Accordingly, for every pixel in the original
image, there are nine pixels in the restoration. From tests on
simulated data, we found this degree of sampling to be ade-
quate to achieve the highest reliable resolution in the images
in a reasonable amount of computing time. The resolution
limits achieved will be discussed in Sec. 4.

In the restored *g* and *r* images, component B appears
slightly, but significantly, more extended than component
A. While the contrast between components is evident in the
grayscale images, the difference is most visible in the insets.
In the *i* band, the restored images of components A and B do
not appear markedly different.

In *g* and *r*, the restored images of component B appear to
be elongated in roughly the direction perpendicular to the
line joining A and B. This result concurs with that of Nieto *et
al.* insofar as at comparable resolutions, approximately 0.4",
they claim to find the very same elongation in their images.
At resolutions on order of 0.26", however, they find B can be
resolved into two sources, B1 and B2, separated by approxi-
mately 0.36" and aligned roughly in the direction of A. One
of the subcomponents, B2, appears to be resolved, they say,
resulting in the perpendicularly elongated appearance of B
at coarser resolutions. Though we fail to detect subcompon-
ents B1 and B2, we do agree with their basic contention that
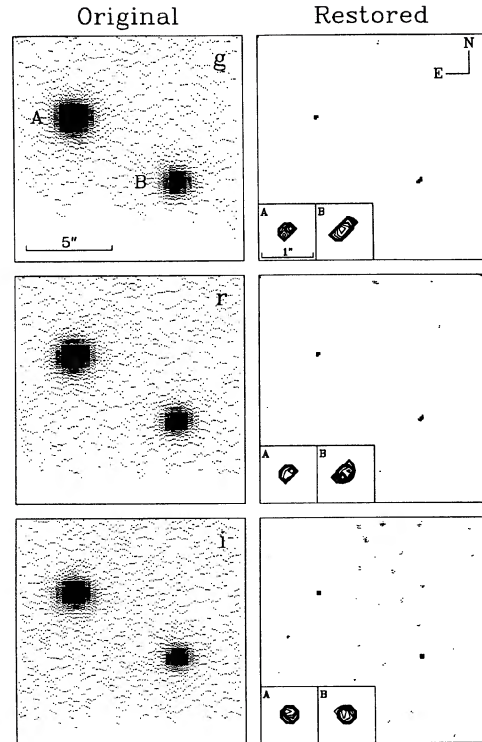at a resolution of about 0.4", component B appears resolved

FIG. 1. Gray-scale plots of original and maximum entropy
restored images of the QSOs in *g*, *r*, and *i*. In the restored
images, black corresponds to 1% of the peak pixel value or
greater. In the insets, components A and B are enlarged by
a factor of 3 relative to the gray-scale plots. The first con-
tour represents 0.25% of the object peak pixel value;
successive contours are at powers of two times this value.
Each image was restored with three times higher spatial
sampling than in the original data, resulting in nine re-
stored image pixels for every one in the original data.

while A is not. As the simulations described in the next sec-
tion show, our data and restoration method would not neces-
sarily allow the detection of structures at the scale of B1 and
B2 in every image we observed. Nonetheless, we find it sur-
prising that we do not find evidence for significant extension
in the direction of B1 and B2 in any of our three images.

4. SIMULATIONS AND TESTS

In order to estimate the reliability and power of our decon-
volution method as applied to these data, we performed ex-
tensive restorations of simulated images. We had performed
extensive tests on our maximum entropy system prior to
analyzing these images, but we found that these data suf-
fered from a particular problem we had not encountered or
simulated properly before. Due to irregularities in the optics
of the 4-Shooter camera, the PSF varies slightly across the
chip. In the case of our images, the only stars available for
estimating the PSF were far enough from the QSOs that they
failed to precisely represent the PSF for the objects. Such a
mismatch in the real and estimated PSF obviously has an
effect on the degree of resolution achievable in any deconvo-
lution method. We determined that this mismatching prob-
lem was the primary factor limiting the super-resolution ca-

pabilities of our method for these images. Nonetheless, we found the method to still be very robust and accurate in detecting structure at small scales, albeit less powerful than in the case where the PSF is perfectly well known.

We chose to model the *g* band data because they indicated the most extended structure for component B, and therefore, in our opinion, warranted particular scrutiny. To appropriately model these data, we first required that the total magnitude of our simulated components A and B equal the instrumental magnitude of these components in the real data. In our model images, however, each component was given a 50% probability of actually consisting of two subcomponents whose relative intensities were randomly chosen from a uniform distribution of 0.05:1 to 0.95:1. The *x* and *y* coordinates of each component or subcomponent were randomly chosen from uniform distributions two pixels wide and centered on the centroid locations of objects A and B in the real data image. With these constraints, we blindly created 50 random representations of components A and B, either one of which could either be a single or double.

To create simulated data images from these model images, we first needed an estimate of the PSF in the *g* image. To do so, we assumed component A was unresolved at a sufficiently small scale to adequately represent the true PSF. By fitting isophotal magnitude ellipses to the image, we were able to create a smooth version of A while still preserving its major asymmetries. This PSF was then used to convolve the point sources in the 50 model images to create appropriately blurred data images, to which the appropriate sky, Poisson noise and additive Gaussian read-out noise were added to simulate the real *g* data.

To restore these simulated images, we also required an (necessarily inaccurate) estimate of the PSF comparable to the one used to restore the real data. To do so, we fit ellipses to the PSF derived from the actual *g* band CCD frame. Using this smooth estimate of the PSF, we created a fake frame containing three stars with different magnitudes and subpixel centroids. A sky background and noise were added to the frame in the same manner as for the object images. We next ran DAOPHOT on this simulated CCD image to create a new PSF estimate, in exactly the same manner as for the real data.

We then restored the 50 simulated images using this simulated PSF estimate. Since our deconvolution method has a clearly defined stopping criterion, we were able to restore these images in batch mode without any subjective interaction.

For the first 25 test images, we analyzed the resulting restorations with knowledge of the number, magnitude, and position of the sources used to create the image. With this training set, we were able to determine the limits of our method and the criterion for distinguishing resolved from unresolved sources. The rule we derived was in fact quite simple: if the restored object appeared extended for more than two pixels in any direction at a flux level of 0.5% of the peak value or above, the object could safely be categorized as resolved. Using this criterion on all 50 images, where the second 25 were categorized in a completely blind fashion, we did not once classify any of the 49 isolated point sources in the simulated images as extended. We were, however, unable to resolve many images which contained real substructure. In other words, if we concluded that an image was a composite using our criterion, it almost certainly was, and any misclassifications were always in the conservative sense. Our resolution ability is summarized in the plots in Fig. 2. In each, we plot the relative intensity and pixel separation of all the subcomponent pairs in the simulated images. A filled square indicates that the object was resolved using our criterion; an open one means that it was not. Figure 2(a) corresponds to subcomponents which comprised component A in our simulated images, where the average peak pixel signal-to-noise ratio (S/N) was approximately 137. Figure 2(b) is for those subcomponents which made up component B, with a peak S/N of roughly 60. Note that while no sharp division can be drawn in these planes distinguishing those objects which were or were not resolvable, there does seem to be a clear trend that the higher the S/N of the data, the larger the area of this parameter space which is within the resolution limit of our method. The dashed line in each plot qualitatively suggests this limit for these two S/N regimes. In general, we find the potential resolving power of the method increases with S/N, though its consistency may not. Thus, while a particular realization of an image of a composite object may not be resolvable from one image to the next, if it is truly a point source, it will not be classified otherwise at least 98% of the time.

In Fig. 3, we show two example simulated images. The first, Fig. 3(a), consists of two point sources, and virtually all the flux in each of the two components in the restored image is located in a small triangle of three pixels. The vast
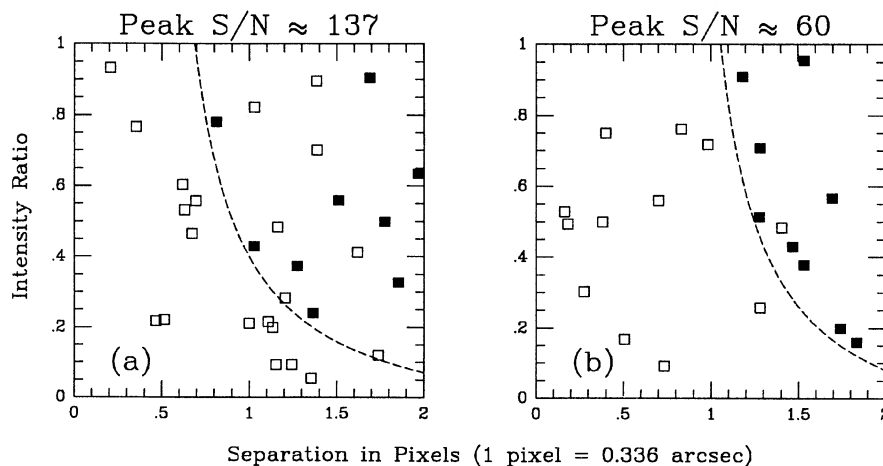

FIG. 2. Separation and intensity ratio of subcomponents comprising component A (a) and B (b) in the simulated images. Filled squares indicate those objects resolved by our restoration method, open squares those that were not. The dashed lines qualitatively suggest the limiting resolving power of the method in the two S/N regimes.
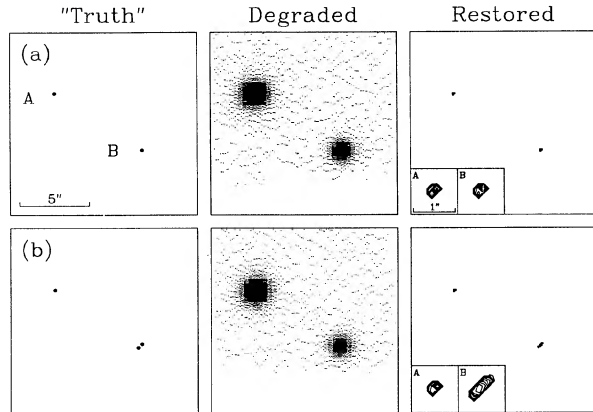
Separation in Pixels (1 pixel = 0.336 arcsec)

FIG. 3. Gray-scale plots of two simulated images, the degraded data images derived from them, and their restorations: (a) two point sources; (b) three point sources, two of which are of equal intensity and separated by 1.13 pixels = 0.38". Pixel sizes, gray scales, and contour levels are the same as described in Fig. 1.

majority of all the point sources in our simulated images, regardless of their original subpixel locations, restored to configurations exactly like this, with an occasional few occupying only two pixels or, in some cases, a square of four. Note the agreement with component A in the real data. Figure 3(b) is a simulated image where component B consists of two subcomponents of equal magnitude separated by just over a single pixel's width. The restoration of this object is clearly distinguishable from that of a point source.

5. PHYSICAL INTERPRETATION

Based upon our simulation results, we conclude that our detection of elongation of component B in the g and r bands in real and, to the limited extent mentioned in Sec. 3, consistent with the findings of Nieto *et al.* The lack of detection of extension in the i band is inconclusive, and it may or may not indicate a different morphology of component B in this band. The degree of substructure inferred from our g and r restorations, and from the Nieto *et al.* results, is of a sufficiently small nature that we might expect not to see it in a fraction of our images. The fact that component A appears unresolved in all three bands, however, does imply that it probably does not contain structure at about the 1.2 pixel level ($\approx 0.4''$) up to intensity ratios of about 5:1 or less.

While Nieto *et al.* interpreted their images to lend support to the gravitational lens hypothesis for the quasars, we are led to exactly the opposite conclusion. In the simplest practical case of a single lensing object with an elliptical gravitational potential and finite core size, the resulting number of observed images should be odd, and the two most closely spaced components, if aligned in the tangential direction, should be the brightest (see, e.g., Blandford & Kochanek 1987). If we assume component B consists of two images aligned in the tangential direction, the same direction of extension which we observe, the intensity ratio of A and B is obviously in the wrong sense. If B splits in the radial direction, however, as Nieto *et al.* claim but we fail to confirm, the observed flux ratio of A to B is consistent with theory for a single elliptical gravitational potential (Blandford & Kochanek 1987). Nieto *et al.* proposed that the A and B splitting may result from the action of a galaxy, its cluster and

associated dark matter at $z \approx 1.5$, with the additional splitting of B (into B1 and the extended or multicomponent B2) by yet another galaxy in the same cluster. While these and other more elaborate configurations might be contrived to explain the images via lensing, the more natural explanation in our opinion is that A and B are two physically independent quasars. Such quasar or active galactic nuclei pairs at high redshift are in fact now known to exist: PKS 1614 + 051 (Djorgovski *et al.* 1985, 1987a), PKS 1145 − 071 (Djorgovski *et al.* 1987b), QQ 1343 + 266 (Crampton *et al.* 1988), and PHL 1222 (Meylan *et al.* 1990a,b). The lack of an observed lensing galaxy (Tyson *et al.* 1986), the significant differences in the spectra (Steidel & Sargent 1990), and the configuration of the image components are all consistent with a similar interpretation of QQ 2345 + 007.

As yet, we are unable to interpret the physical cause of the elongation of component B. Clearly more and higher resolution data are required in order to determine the true morphology of the object and ascertain whether there are any significant differences at different wavelengths. Such measurements, for example, would help to clarify whether we are seeing a galaxy underlying or along the sight of component B and causing the perpendicular elongation.

The observed color difference and magnitude difference variability between components A and B is interesting, but provides ambiguous information as to possible physical scenarios. The redder appearance of B may be due to an underlying or intervening galaxy, but not necessarily one acting as a lens. Variability in the intensity ratio would be expected for either the gravitational lens or the binary quasar interpretation.

The significant discrepancy between our and Steidel and Sargent's (1990) magnitude difference measurement at virtually the same epoch may most likely be explained as an artifact of their observational method. In particular, a combination of small slit width and the extended nature of component B would conspire to make their spectroscopically measured magnitude difference highly sensitive to slit placement and position angle. To gauge this sensitivity, we convolved our restored g image with a Gaussian of FWHM $\approx 0.9''$ to stimulate the seeing conditions reported by them. Prior to convolution, we also slightly scaled component A so that the magnitude difference in the restored image exactly matched that which we measured in the original data, $\Delta m = 1.32$. We then calculated the flux ratio which would be measured in a 1.0" slit passing over A and B, integrating 1.0" along the slit over each object. If we placed the slit precisely on the centroid of A, but off 2 ° from the nominal position angle (P. A.) of 237 °, the measured Δm was 1.47. If we used the correct P. A., but centered the slit 0.3" from the centroid of A, we measured a Δm as high as 1.40. A slight misalignment of the slit relative to the two components would therefore easily account for the difference between our measurements and those of Steidel and Sargent.

6. CONCLUSION

We have presented high-resolution images and differential photometry of the intriguing QSO pair 2345 + 007A,B. We have also demonstrated the usefulness of a powerful new deconvolution technique in the morphological analysis of objects at the highest possible spatial resolution. We find that in two of the three QSO images we restored, there is

clear evidence for elongation of component B, in partial agreement with the claims of Nieto *et al.* (1988). We are not able to detect subcomponents of B aligned in the direction joining A and B. Although the resolving power of our image restoration method varies for different realizations of even the same image, we find we can usually detect bright substructure at just greater than the pixel ($\approx 0.4''$) level. In all three of our images, we find no evidence for substructure in component A. We find evidence that component B is redder than component A, and that the magnitude difference between the two may be variable. While these and recent spectroscopic observations do not rule out the possibility of grav-itational lensing, we believe the objects may more easily be explained as a binary quasar association.

REFERENCES

Blandford, R. D, and Kochanek, C. S. 1987, ApJ, 321, 658

Crampton, D., Cowley, A. P., Hickson, P., Kindl, E., Wagner, R. M., Tyson, J. A., and Gullixson, C. 1988, ApJ, 330, 184

Djorgovski, S., Perley, R., Meylan, G., and McCarthy, P. 1987b, ApJ, 321, L17

Djorgovski, S., Spinrad, H., McCarthy, P., and Strauss, M. 1985, ApJ, 299, L1

Djorgovski, S., Strauss, M., Perley, R., Spinrad, H., and McCarthy, P. 1987a, AJ, 93, 1318

Foltz, C. B., Weymann, R. J., Roser, H-J., and Chaffee, F. H. 1984, ApJ, 281, L1

Gull, S. F. 1989, in Maximum Entropy and Bayesian Methods, edited by J. Skilling (Kluwer, Dordrecht), p. 53

Gull, S. F., and Skilling, J. 1989, Quantified Maximum Entropy "MEMSYS 3" Users' Manual

Meylan, G., Djorgovski, S., Weir, N., and Shaver, P. 1990a, in Gravitational Lensing, Lecture Notes in Physics 360, edited by Y. Mellier, B. Fort, and G. Soucail (Springer, Berlin)

Meylan, G., Djorgovski, S., Weir, N., and Shaver, P. 1990b, ESO Messenger, No. 59, edited by R. M. West (European Southern Observatory, Garching bei München), p. 47

Nieto, J. L., Roques, S., Llebaria, A., Vanderriest, C., Lelievre, G., Di Serego Alighieri, S., Macchetto, F. D., and Perryman, M. A. C. 1988, ApJ, 325, 644

Schild, R., Weir, N., and Matthieu, R. D. 1989, AJ, 97, 1110

Skilling, J., 1989 in Maximum Entropy and Bayesian Methods, edited by J. Skilling (Kluwer, Dordrecht)

Sol, H., Vanderriest, C., Lelievre, G. Pedersen, H., and Schneider, J. 1984, A&A, 132,105

Steidel, C. C., and Sargent, W. L. W. 1990, AJ, 99, 1693

Stetson, P. 1987, PASP, 99, 191

Tyson, J. A., Seitzer, P., Weymann, R. J., and Foltz, C. 1986, AJ, 91, 1274

Weedman, D. W., Weymann, R. J., Green, R. F., and Heckman, T. M. 1982, ApJ, 255, L5

Weir, N. 1987, Senior thesis, Harvard University

Weir, N. 1991, in preparation